Available online at www.sciencedirect.com

ScienceDirect

Nuclear Physics A 992 (2019) 121624

NUCLEAR PHYSICS A

www.elsevier.com/locate/nuclphysa

Spin-dependent WIMP-nucleus scattering off ^{125}Te, ^{129}Xe, and ^{131}Xe in the microscopic interacting boson-fermion model

P. Pirinen [a,*], J. Kotila [b,c], J. Suhonen [a]

[a] *University of Jyvaskyla, Department of Physics, P. O. Box 35 (YFL), FI-40014, Finland*
[b] *Finnish Institute for Educational Research, University of Jyväskylä, P.O. Box 35, FI-40014 Jyväskylä, Finland*
[c] *Center for Theoretical Physics, Sloane Physics Laboratory, Yale University, New Haven, CT 06520-8120, USA*

Received 19 August 2019; accepted 4 September 2019
Available online 10 September 2019

Abstract

We perform calculations of structure functions for elastic and inelastic spin-dependent scattering of weakly interacting massive particles (WIMPs) off ^{125}Te, ^{129}Xe, and ^{131}Xe. The nuclear structure calculations are performed in the microscopic interacting boson-fermion model (IBFM-2). In our calculations we employ one-body and leading long-range two-body WIMP-nucleus currents derived from chiral effective field theory. We demonstrate that the relevant matrix elements can be reliably computed in the IBFM-2, which will allow investigation of heavy deformed nuclei previously inaccessible to theoretical calculations.

Keywords: Dark matter; WIMP; Scattering; Interacting boson-fermion model; Nuclear structure

1. Introduction

To this day, we do not know what most of our Universe is made of. Based on cosmic microwave background measurements [1,2], observations of galactic rotation curves [3–6], studies of structure formation [7,8], backed up by the Bullet Cluster observations, a nonbaryonic cold

* Corresponding author.
E-mail address: pekka.a.pirinen@jyu.fi (P. Pirinen).

https://doi.org/10.1016/j.nuclphysa.2019.121624

dark matter component that forms roughly 80% of all matter is required. The problem of dark matter still continues to puzzle scientists, and efforts to finally find the majority of matter in our Universe grow ever stronger.

If dark matter consists mainly of weakly interacting massive particles (WIMPs), directly detecting the interaction of a WIMP with an atomic nucleus would be an excellent probe to the properties of dark matter [9]. We will assume the WIMPs have a nonzero spin (spin 1/2 in this work), and we focus on spin-dependent WIMP-nucleus scattering [10]. Analyzing detector signals of spin-dependent WIMP-nucleus scattering requires detailed information of the nuclear structure of the target nucleus in form of structure functions. Computing these structure functions requires a reliable microscopic model of the nucleus.

Calculations of structure functions for WIMP-nucleus scattering have typically been performed in the nuclear shell model [11–22]. However, heavy target nuclei far away from closed shells present a challenge for the shell model. Here we consider a different approach in the microscopic interacting boson-fermion model (IBFM-2). The IBFM-2 models heavy nuclei and deformed nuclei well by design [23]. To our knowledge, only one calculation exists in the early years of WIMP-nucleus scattering studies, where ground-state spin expectation values for a range of nuclei were calculated in the IBFM [24]. The analysis of Ref. [24] was as such limited to zero momentum transfer. Our aim in this paper is to demonstrate that the IBFM-2 can be used to reliably compute structure functions for heavy nuclei used in dark matter direct detection by comparing calculations for ^{125}Te, ^{129}Xe, and ^{131}Xe to earlier benchmark shell-model calculations in the literature. The IBFM-2 approach can then be used to gain information on deformed heavy nuclei used in dark matter detectors, such as ^{183}W in the CRESST detector [25].

Axial-vector WIMP-nucleus currents were derived in the framework of chiral effective field theory (chiral EFT) in Refs. [11,12]. In addition to the conventional one-body currents [10], Refs. [11,12] were able to include the leading long-range two-body currents, which turned out to have a noticeable effect on the structure functions of spin-dependent WIMP-nucleus scattering. In Ref. [13] the analysis was extended to inelastic scattering of WIMPs off the odd-mass xenons. In the present work we employ the axial-vector WIMP-nucleus currents from chiral EFT, and show results for combined one and two-body currents along with results computed with one-body currents only.

This article is organized as follows. In Section 2 we outline the formalism for computing the axial-vector structure functions for spin-dependent WIMP-nucleus scattering. In Section 3 the details of the performed IBFM-2 calculation are given. In Section 4 we discuss our main results, and finally we summarize and draw conclusions in Section 5.

2. Structure functions

The spin-dependent WIMP-nucleus cross section can be written as [10]

$$\frac{d\sigma}{dq^2} = \frac{8G_F^2}{(2J_i+1)v^2} S_A(q), \tag{1}$$

where G_F is the Fermi coupling constant, v is the speed of the WIMP in the laboratory frame, and q is the momentum transfer from the nucleus to the WIMP. S_A is the axial-vector structure factor which can be expressed as a multipole decomposition as

$$S_A(q) = \sum_{L\geq 0} \left| \langle J_f || \mathcal{L}_L^5(q) || J_i \rangle \right|^2$$

$$+\sum_{L\geq 1}\left(\left|\langle J_f||\mathcal{T}^{\mathrm{el5}}_L(q)||J_i\rangle\right|^2+\left|\langle J_f||\mathcal{T}^{\mathrm{mag5}}_L(q)||J_i\rangle\right|^2\right). \tag{2}$$

Here we have

$$\mathcal{L}^5_L(q)=\frac{i}{\sqrt{2L+1}}\sum_{i=1}^{A}\frac{1}{2}\left[a_0+a_1\tau_i^3\left(1+\delta a_1(q)-\frac{2g_{\pi\mathrm{pn}}F_\pi q^2}{2m_{\mathrm{p}}g_{\mathrm{A}}(q^2+m_\pi^2)}+\delta a_1^{\mathrm{P}}(q)\right)\right]$$
$$\times\left[\sqrt{L+1}M_{L,L+1}(q\mathbf{r}_i)+\sqrt{L}M_{L,L-1}(q\mathbf{r}_i)\right], \tag{3}$$

$$\mathcal{T}^{\mathrm{el5}}_L(q)=\frac{i}{\sqrt{2L+1}}\sum_{i=1}^{A}\frac{1}{2}\left[a_0+a_1\tau_i^3\left(1-\frac{2q^2}{\Lambda_{\mathrm{A}}^2}+\delta a_1(q)\right)\right]$$
$$\times\left[-\sqrt{L}M_{L,L+1}(q\mathbf{r}_i)+\sqrt{L+1}M_{L,L-1}(q\mathbf{r}_i)\right], \tag{4}$$

and

$$\mathcal{T}^{\mathrm{mag5}}_L(q)=\frac{i}{\sqrt{2L+1}}\sum_{i=1}^{A}\frac{1}{2}\left[a_0+a_1\tau_i^3\left(1-\frac{2q^2}{\Lambda_{\mathrm{A}}^2}+\delta a_1(q)\right)\right]M_{L,L}(q\mathbf{r}_i), \tag{5}$$

where $F_\pi=92.4$ MeV is the pion decay constant, $m_\pi=138.04$ MeV the pion mass, $m_{\mathrm{p}}=938.27$ MeV the proton mass, $\Lambda_{\mathrm{A}}=1040$ MeV the axial mass scale, $g_{\mathrm{A}}=1.26$ the axial-vector coupling constant, and $g_{\pi\mathrm{pn}}=13.05$ the strong pion-nucleon coupling constant [12]. The operator $M_{L,L'}$ is defined as $M_{L,L'}=j_{L'}(qr_i)[Y_{L'}(\hat{\mathbf{r}}_\mathbf{i})\boldsymbol{\sigma}_i]_L$, where $j_{L'}$ is a Bessel function, $Y_{L'}$ a spherical harmonic, and σ a Pauli spin operator.

The effect of two-body currents from chiral EFT enters the structure functions (3)–(5) in the coefficients $\delta a_1(q)$ and $\delta a_1^{\mathrm{P}}(q)$. They are defined as [12]

$$\delta a_1(q)=-\frac{\rho}{F_\pi^2}\left[\frac{1}{3}\left(c_4+\frac{1}{4m_{\mathrm{p}}}\right)\left[3I_2^\sigma(\rho,q)-I_1^\sigma(\rho,q)\right]\right.$$
$$\left.+\frac{1}{3}\left(-c_3+\frac{1}{4m_{\mathrm{p}}}\right)I_1^\sigma(\rho,q)-\left(\frac{1+\hat{c}_6}{12m_{\mathrm{p}}}\right)I_{c6}(\rho,q)\right] \tag{6}$$

and

$$\delta a_1^{\mathrm{P}}(q)=\frac{\rho}{F_\pi^2}\left[\frac{-2c_3q^2}{m_\pi^2+q^2}+\frac{c_3+c_4}{3}I^{\mathrm{P}}(\rho,q)+\frac{1+\hat{c}_6}{12m_{\mathrm{p}}}I_{c6}(\rho,q)\right]. \tag{7}$$

For details about the integrals I_1^σ, I_2^σ, I_{c6}, and I^{P}, and the formalism in general, see Ref. [12].

We follow the choices of Ref. [12] for the values of low-energy couplings c_3, c_4, and $\hat{c}_6$. We thus take $\hat{c}_6=5.83$ [26], and a range of values of $c_3=-2.2\ldots-4.78\,\mathrm{GeV}^{-1}$ and $c_4=2.4\ldots5.4\,\mathrm{GeV}^{-1}$ combined from Refs. [27–30]. For the density we adopt the range of values $\rho=0.10\ldots0.12\,\mathrm{fm}^{-3}$. It should be noted that the dependence of our results on variation of the parameter $\hat{c}_6$ is very mild and it only affects the structure functions at quite high q. Therefore we neglect the uncertainty in this parameter as the uncertainties in c_3 and c_4 are much more significant.

Table 1
Boson-fermion interaction parameters (MeV).

Nucleus	Γ_ρ	Λ_ρ	A_ρ
^{125}Te	1.2	0.04	−0.76
^{129}Xe	0.85	0.28	−0.38
^{131}Xe	0.51	0.32	−0.495

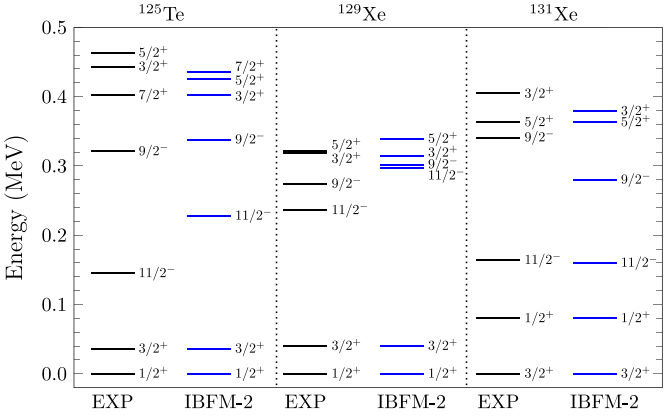

Fig. 1. Experimental and computed energy levels of (from left to right) ^{125}Te, ^{129}Xe, and ^{131}Xe.

3. IBFM-2 calculation

For the IBFM-2 calculation even-even ^{126}Te, ^{130}Xe and ^{132}Xe nuclei were used as core to the odd ^{125}Te, ^{129}Xe and ^{131}Xe nuclei, respectively. The parameters for the core Xe nuclei were taken from Ref. [31] with following modifications for A=130: $\xi_1 = 0.12$, $c_2^\nu = 0.00$ and for A=132: $\kappa = -0.10$, $\chi_\nu = 0.6$, $\xi_1 = 0.12$, $c_4^\nu = -0.131$. For the Te core nucleus the starting parameters were taken from Ref. [32] and modified as $\epsilon = 0.72$, $\kappa = -0.03$, $\xi_1 = \xi_3 = 0.00$, $\xi_2 = 0.25$, $c_0^\nu = 0.6$. The valence space was chosen to span the $0g_{7/2}$, $1d_{5/2}$, $1d_{3/2}$, $2s_{1/2}$ and $0h_{11/2}$ proton and neutron orbitals with unperturbed single particle energies taken from [33], where the effect of single particle energies to occupation probabilities was studied. The used boson-fermion interaction parameters are listed in Table 1.

The mapping of the single fermion creation operator onto the IBFM space follows the procedure introduced in Ref. [34] where evaluation of the relevant terms using exact values for the fermion matrix elements in the Generalized Seniority scheme was worked out and use of Number Operator Approximation (NOA) is avoided. For the even numbered nucleons, protons in the cases of interest here, the mapping procedure from the shell model into the microscopic IBM is described in detail in Refs. [35,36] and more recently in Ref. [37] in connection with studies of double beta decay and in Ref. [33] for calculating occupation probabilities. Basically, the shell-model creation operators of collective pairs of angular momenta 0 and 2, the S and D pairs of interest here, are used to span the SD fermion space, which is a subspace of the full shell model space. The states of the SD subspace are then mapped onto boson states belonging to the IBM space.

In Fig. 1 we show the experimental and calculated low-lying energy spectra of ^{125}Te, ^{129}Xe, and ^{131}Xe. The energy of the first excited state is fitted exactly to the experimental value by the

interaction parameters. The correspondence between calculated and experimental energy levels is quite good, especially for the positive-parity states.

4. Results

We express our results for structure functions S_A as a function of the momentum transfer in a dimensionless form $u = b^2q^2/2$, where b is the harmonic oscillator length. We use a decomposition to isoscalar and isovector parts:

$$S_A(u) = a_0^2 S_{00}(u) + a_0 a_1 S_{01}(u) + a_1^2 S_{11}(u). \tag{8}$$

For the convenience of experiments, we present our results in form of so called proton-only ($a_0 = a_1 = 1$) and neutron-only ($a_0 = -a_1 = 1$) couplings:

$$S_p(u) = S_{00}(u) + S_{01}(u) + S_{11}(u), \tag{9}$$

$$S_n(u) = S_{00}(u) - S_{01}(u) + S_{11}(u). \tag{10}$$

We will start by discussing some key magnetic properties of the target nuclei. The ground-state spin expectation values $\langle S_p \rangle$ and $\langle S_n \rangle$ determine the spin structure function S_A for elastic scattering at zero momentum transfer:

$$S_A(0) = \frac{(2J+1)(J+1)}{4\pi J} \left| (a_0 + a_1 + \delta a_1(0))\langle S_p \rangle + (a_0 - a_1 - \delta a_1(0))\langle S_n \rangle \right|^2. \tag{11}$$

The magnetic dipole moment of the ground state and the $M1$ transition strength from the first excited state to the ground state involve the spin operator, and therefore these quantities can be used to give a rough idea of how the modeling error in our nuclear structure calculations might carry over to the WIMP-nucleus scattering results of elastic and inelastic scattering, respectively.

In Table 2 we present the computed spin expectation values for protons and neutrons in the ground state along with the computed and experimental ground-state magnetic moments for each of our target nuclei. We also compare our values with earlier shell-model calculations and the IBFM calculation of Ref. [24]. The spin expectation values for neutrons computed in the present work are in general smaller than in earlier shell-model calculations. It should be noted that the simplified IBFM calculation of Ref. [24] gives spin expectation values quite close to one-particle estimates, which accounts for the values being considerably larger than those computed in the present work. In Ref. [21] the computed ground-state magnetic moment for ^{125}Te was overestimated much more than in the present IBFM-2 calculation. Therefore the magnetic properties of the ground state are likely to be better represented by the present calculation. Our calculation for ^{125}Te is much more in line with the results of Ref. [15]. For the xenons our magnetic moments are in decent agreement with experiment, although the magnetic moment is slightly overestimated for ^{131}Xe. In Ref. [11] the ground-state magnetic moments for the xenons were computed using effective g factors, which yielded a good agreement with the experimental values. In the present work we used bare g factors, which makes a direct comparison between the magnetic moment calculations difficult.

In Table 3 we show the calculated and experimental $B(M1)$ transition strengths for the transition from the lowest excited state to the ground state for each of our target nuclei. For ^{131}Xe the calculated value lies only slightly below the experimental lower limit. For ^{129}Xe and especially ^{125}Te the calculated values are significantly smaller than the experimental values. A somewhat similar difference between calculated and experimental B(M1) value for ^{125}Te was obtained in

Table 2
Ground-state spin expectation values and ground-state magnetic moments for ^{125}Te, ^{129}Xe, and ^{131}Xe. The calculations were made using bare magnetic g factors, i.e., $g_{s,n} = -3.826$, $g_{s,p} = 5.586$, $g_{l,n} = 0$, and $g_{l,p} = 1$. The results of the present calculation are compared to earlier shell model (SM) and interacting boson-fermion model (IBFM) calculations. The experimental data of column 6 was read from Ref. [38].

Nucleus	Calculation	$\langle S_p \rangle$	$\langle S_n \rangle$	μ_{gs}^{th} (μ_N)	μ_{gs}^{exp} (μ_N)
^{125}Te	Present IBFM-2	−0.00008	0.266	−1.017	−0.8885051(4)
	SM [21]	−0.00663	0.427	−1.598	
	SM [15] a)	0.001	0.287	−1.015	
	SM [15] b)	−0.003	0.323	−1.134	
	IBFM [24]	−0.0008	0.499		
^{129}Xe	Present IBFM-2	−0.0078	0.216	−0.765	−0.7779763(84)
	SM [11,12]	0.010	0.329		
	SM [19]	−0.0019	0.273	−0.94	
	SM [15] a)	0.028	0.359	−0.983	
	SM [15] b)	0.0128	0.300	−0.701	
	IBFM [24]	0.000	0.430		
^{131}Xe	Present IBFM-2	−0.0222	−0.188	+0.896	+0.691862(4)
	SM [11,12]	−0.009	−0.272		
	SM [19]	−0.00069	−0.125	+0.72	
	SM [15] a)	−0.009	−0.227	+0.980	
	SM [15] b)	−0.012	−0.217	+0.979	
	IBFM [24]	0.000	−0.277		

Table 3
Calculated (column 3) and experimental (column 4) M1 transition strengths $B(M1)$ for the transition from the first excited state to the ground state for ^{125}Te, ^{129}Xe, and ^{131}Xe. The calculations were made using bare magnetic g factors, i.e., $g_{s,n} = -3.826$, $g_{s,p} = 5.586$, $g_{l,n} = 0$, and $g_{l,p} = 1$. The experimental data was read from Ref. [38]. The values are given in Weisskopf units.

Nucleus	Calculation	$B(M1)$ (W.u.)	
		th	exp
^{125}Te	Present IBFM-2	0.0018	0.0226(4)
	SM [21]	0.0056	
^{129}Xe	Present IBFM-2	0.0068	0.0281(7)
	SM [19]	0.023	
^{131}Xe	Present IBFM-2	0.034	> 0.057
	SM [19]	0.033	

the shell-model calculation of Ref. [21]. In both this work and Ref. [21] the structure functions for inelastic WIMP-nucleus scattering might thus be underestimated for ^{125}Te.

Here it should be noted that the magnetic moment and $B(M1)$ values do not probe exactly the same physics that is involved in WIMP-nucleus scattering. However, the involved operators are similar, and as possibilities for systematic error analysis are limited in these kinds of calculations, we take the opportunity to use whatever measure of accuracy that is available. One could in principle find effective g factors to improve agreement with experiment for the magnetic moments and $B(M1)$ values, and then renormalize the spin operator accordingly to deliver the effect into the axial-vector structure functions. This approach has been taken in Ref. [19].

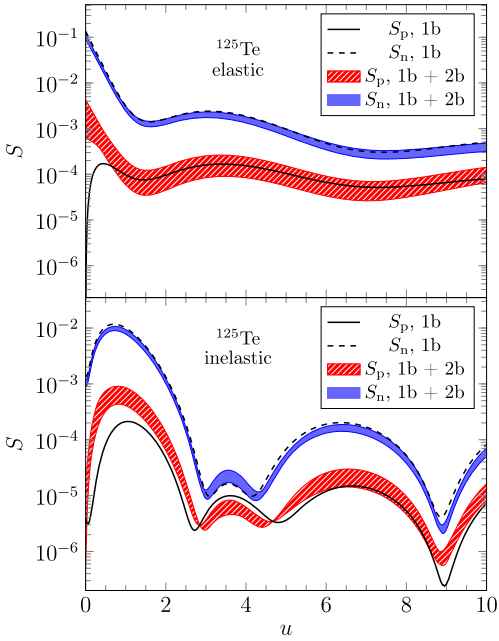

Fig. 2. (Color online.) Proton-only and neutron-only spin structure functions S_p and S_n for elastic (upper panel) and inelastic (lower panel) scattering for ^{125}Te. Results are shown for one-body currents only as solid (S_p) and dashed (S_n) lines as well as for two-body currents as red striped (S_p) and blue (S_n) bands. The thickness in the two-body current results represent the uncertainty in the low-energy couplings c_3, c_4, and the density ρ.

However, we choose to use the bare g factors due to the ambiguity related to choosing suitable effective g factors and the fact that there is no guarantee that the renormalization should be the same for WIMP-nucleus interactions.

The proton-only and neutron-only spin structure functions of Eqs. (9) and (10) for ^{125}Te, ^{129}Xe, and ^{131}Xe are shown in Figs. 2, 3, and 4, respectively. We show results with and without the two-body current contributions. In our calculations we include the uncertainty arising from the unknown values of the c_3 and c_4 low-energy couplings as well as the density ρ in the two-body contributions of Eqs. (6) and (7) as discussed in Section 2. The uncertainties are represented by colored error bands in our figures, and the bands correspond to values of $c_3 = -2.2 \ldots -4.78\,\mathrm{GeV}^{-1}$ and $c_4 = 2.4 \ldots 5.4\,\mathrm{GeV}^{-1}$, and $\rho = 0.10 \ldots 0.12\,\mathrm{fm}^{-3}$.

For ^{125}Te we can compare our results with the shell-model calculations of Ref. [21]. The formalism of Ref. [21] is somewhat different than the one used in this work in that only one-body axial-vector currents were included and the structure functions were normalized to unity at zero momentum transfer. Translated to the S-function formalism of the present work we note that the structure functions of [21] are larger in magnitude than the structure functions computed in the present work for both elastic and inelastic scattering. This is consistent with the larger computed ground-state magnetic moment and first excited state to ground state $B(M1)$ values of Tables 2 and 3. The elastic scattering results of the present work could be considered more accurate than the results of [21] as the ground-state magnetic moment is in better agreement with experiment. The present calculation yields a worse agreement with experiment in the $B(M1)$ values, though,

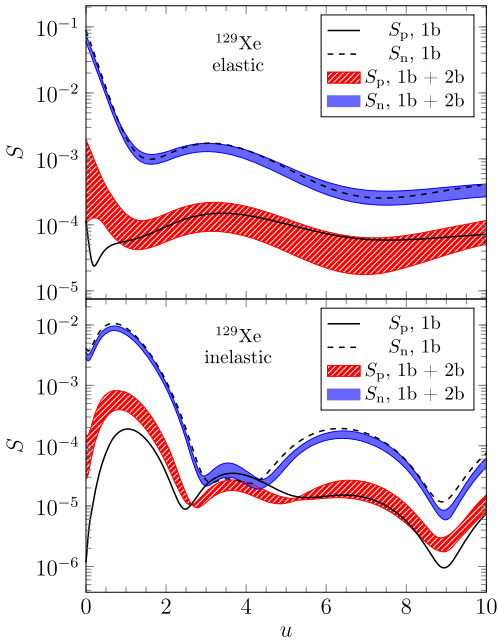

Fig. 3. (Color online.) Same as Fig. 2, but for ^{129}Xe.

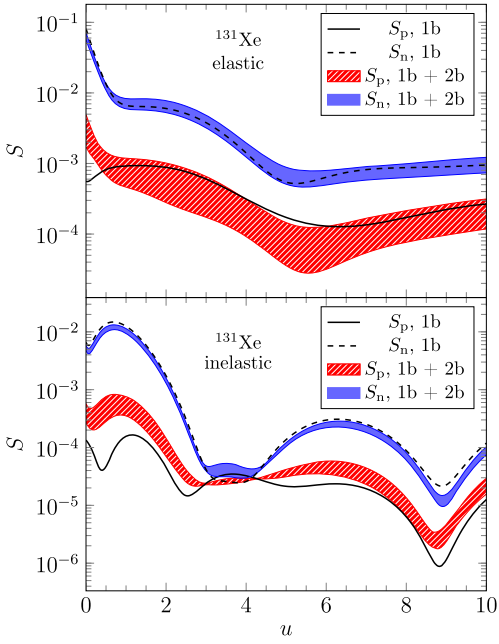

Fig. 4. (Color online.) Same as Fig. 2, but for ^{131}Xe.

and the structure functions for inelastic scattering are likely to be underestimated as mentioned earlier.

The benchmark to compare our results for the xenons is the shell-model calculation of Refs. [11,12] in the elastic channel and [13] in the inelastic channel. The structure functions for elastic scattering computed in the present work are smaller than those of Refs. [11,12] as anticipated by the smaller spin expectation values in Table 2. The shape of our structure functions is mostly very similar to the structure functions of Refs. [11–13], but in the proton-only structure functions $S_{\rm p}$ in the inelastic channel there are some notable differences. The inelastic $S_{\rm p}$ functions in the present work are more flat than those of Ref. [13] and at $u = 0$ they are notably smaller for ^{129}Xe and larger for ^{131}Xe.

Typically one would expect the structure function of the even species of nucleons to get a boost at small u when two-body currents are included into the calculation, due to contributions from the odd species via two-body currents [12,13]. For ^{125}Te and ^{131}Xe this holds true in our calculations. However, for ^{129}Xe the effect of two-body currents at $u = 0$ varies greatly depending on the values of the low-energy couplings c_3 and c_4, and for some choices of the parameters the two-body result is even slightly smaller than the one-body-only result. We noted that for some choices of the IBFM interaction parameters the effect is a lot more pronounced, but such choices also yield worse correspondence with experimental values in both the energy spectrum and ground-state magnetic moment. The behavior of the $S_{\rm p}$ function seems to be quite sensitive to the underlying nuclear structure and the reduced one-body transition density within the proton orbital $0g_{7/2}$. Our IBFM-2 calculation might overestimate that transition density. However, it is difficult to find an unambiguous explanation to the behavior of the $S_{\rm p}$ function.

5. Conclusions

We have computed structure functions for spin dependent WIMP-nucleus scattering in the framework of the microscopic interacting boson-fermion model. Our target nuclei were ^{125}Te, which has enjoyed recent theoretical and experimental interest for inelastic WIMP-nucleus scattering [21,39], and ^{129,131}Xe used in many of the most sensitive current direct detection experiments [40–43]. We have included one-body and two-body WIMP-nucleus currents based on chiral EFT.

The shapes of the structure functions computed in the present work are quite similar to earlier shell-model calculations, especially for the neutron-only couplings $S_{\rm n}$. At zero momentum transfer we obtain the result of earlier works that two-body currents decrease the structure function of the odd-numbered species of nucleons (here $S_{\rm n}$), and increase the structure function for the even-numbered species (here $S_{\rm p}$) compared to the calculation with one-body currents only. ^{129}Xe forms an exception here, as some choices of the low-energy couplings c_3 and c_4 can lead to values of $S_{\rm p}$ that match the one-body-current result at zero momentum transfer. For ^{125}Te we conservatively report more reliable results for elastic scattering than our previous shell-model calculation [21], based on the ground-state magnetic dipole moment in the present work being much closer to the experimental value.

We have demonstrated that the IBFM-2 can be used to quite reliably compute structure functions for WIMP-nucleus scattering. This opens up new opportunities for investigating heavy deformed nuclei for dark matter direct detection. Using the approach of the present work it is possible to perform the first calculation of spin-dependent WIMP-nucleus scattering structure functions for the heavy ^{183}W used currently in the CRESST dark matter detector [25]. In the

future it will also be interesting to investigate structure functions in the general non-relativistic effective field theory developed in Refs. [22,44].

Acknowledgements

This work has been partially supported by the Academy of Finland under the Academy project no. 318043. PP was partially supported by a graduate student stipend from the Magnus Ehrnrooth Foundation. The work of JK was supported by the Academy of Finland (Grant No. 314733).

References

[1] G. Hinshaw, D. Larson, E. Komatsu, D.N. Spergel, C.L. Bennett, J. Dunkley, et al., Nine-year Wilkinson microwave anisotropy probe (WMAP) observations: cosmological parameter results, Astrophys. J. Suppl. Ser. 208 (2) (2013) 19, https://doi.org/10.1088/0067-0049/208/2/19. URL: https://doi.org/10.1088/0067-0049/208/2/19.

[2] P.A.R. Planck Collaboration Ade, N. Aghanim, C. Armitage-Caplan, M. Arnaud, M. Ashdown, et al., Planck 2013 results. XVI. Cosmological parameters, Astron. Astrophys. 571 (2014) A16, https://doi.org/10.1051/0004-6361/201321591. URL: https://doi.org/10.1051/0004-6361/201321591.

[3] F. Zwicky, Die rotverschiebung von extragalaktischen Nebeln, Helv. Phys. Acta 6 (1933) 110–127.

[4] V.C. Rubin, W.K. Ford, Rotation of the Andromeda Nebula from a spectroscopic survey of emission regions, Astrophys. J. 159 (1970) 379–403.

[5] J. Einasto, A. Kaasik, E. Saar, Dynamic evidence on massive coronas of galaxies, Nature 250 (1974) 309–310, https://doi.org/10.1038/250309a0. URL: https://doi.org/10.1038/250309a0.

[6] M.S. Roberts, R.N. Whitehurst, The rotation curve and geometry of M31 at large galactocentric distances, Astrophys. J. 201 (1975) 327–346.

[7] G.R. Blumenthal, S.M. Faber, J.R. Primack, M.J. Rees, Formation of galaxies and large-scale structure with cold dark matter, Nature 311 (1984) 517–525, https://doi.org/10.1038/311517a0. URL: https://doi.org/10.1038/311517a0.

[8] M. Davis, G. Efstathiou, C.S. Frenk, S.D.M. White, The evolution of large-scale structure in a universe dominated by cold dark matter, Astrophys. J. 292 (1985) 371–394.

[9] L. Roszkowski, E.M. Sessolo, S. Trojanowski, WIMP dark matter candidates and searches — current status and future prospects, Rep. Prog. Phys. 81 (6) (2018) 066201, https://doi.org/10.1088/1361-6633/aab913. URL: https://doi.org/10.1088/1361-6633/aab913.

[10] J. Engel, S. Pittel, P. Vogel, Nuclear physics of dark matter detection, Int. J. Mod. Phys. E 01 (01) (1992) 1–37, https://doi.org/10.1142/S0218301392000023. URL: https://doi.org/10.1142/S0218301392000023.

[11] J. Menéndez, D. Gazit, A. Schwenk, Spin-dependent wimp scattering off nuclei, Phys. Rev. D 86 (2012) 103511, https://doi.org/10.1103/PhysRevD.86.103511. URL: https://link.aps.org/doi/10.1103/PhysRevD.86.103511.

[12] P. Klos, J. Menéndez, D. Gazit, A. Schwenk, Large-scale nuclear structure calculations for spin-dependent wimp scattering with chiral effective field theory currents, Phys. Rev. D 88 (2013) 083516, https://doi.org/10.1103/PhysRevD.88.083516. URL: https://link.aps.org/doi/10.1103/PhysRevD.88.083516.

[13] L. Baudis, G. Kessler, P. Klos, R.F. Lang, J. Menéndez, S. Reichard, et al., Signatures of dark matter scattering inelastically off nuclei, Phys. Rev. D 88 (2013) 115014, https://doi.org/10.1103/PhysRevD.88.115014. URL: https://link.aps.org/doi/10.1103/PhysRevD.88.115014.

[14] M.T. Ressell, M.B. Aufderheide, S.D. Bloom, K. Griest, G.J. Mathews, D.A. Resler, Nuclear shell model calculations of neutralino-nucleus cross sections for ^{29}Si and ^{73}Ge, Phys. Rev. D 48 (1993) 5519–5535, https://doi.org/10.1103/PhysRevD.48.5519. URL: https://link.aps.org/doi/10.1103/PhysRevD.48.5519.

[15] M.T. Ressell, D.J. Dean, Spin-dependent neutralino-nucleus scattering for $A \sim 127$ nuclei, Phys. Rev. C 56 (1997) 535–546, https://doi.org/10.1103/PhysRevC.56.535. URL: https://link.aps.org/doi/10.1103/PhysRevC.56.535.

[16] P.C. Divari, T.S. Kosmas, J.D. Vergados, L.D. Skouras, Shell model calculations for light supersymmetric particle scattering off light nuclei, Phys. Rev. C 61 (2000) 054612, https://doi.org/10.1103/PhysRevC.61.054612. URL: https://link.aps.org/doi/10.1103/PhysRevC.61.054612.

[17] E. Holmlund, M. Kortelainen, T. Kosmas, J. Suhonen, J. Toivanen, Microscopic calculation of the LSP detection rates for the 71Ga, 73Ge and 127I dark-matter detectors, Phys. Lett. B 584 (1) (2004) 31–39, https://doi.org/10.1016/j.physletb.2004.01.045. URL: http://www.sciencedirect.com/science/article/pii/S0370269304001789.

[18] M. Kortelainen, T. Kosmas, J. Suhonen, J. Toivanen, Event rates for CDM detectors from large-scale shell-model calculations, Phys. Lett. B 632 (2) (2006) 226–232, https://doi.org/10.1016/j.physletb.2005.10.057. URL: http://www.sciencedirect.com/science/article/pii/S0370269305015467.

[19] P. Toivanen, M. Kortelainen, J. Suhonen, J. Toivanen, Large-scale shell-model calculations of elastic and inelastic scattering rates of lightest supersymmetric particles (LSP) on ^{127}I, ^{129}Xe, ^{131}Xe, and ^{133}Cs nuclei, Phys. Rev. C 79 (2009) 044302, https://doi.org/10.1103/PhysRevC.79.044302. URL: https://link.aps.org/doi/10.1103/PhysRevC.79.044302.

[20] L. Vietze, P. Klos, J. Menéndez, W.C. Haxton, A. Schwenk, Nuclear structure aspects of spin-independent WIMP scattering off xenon, Phys. Rev. D 91 (2015) 043520, https://doi.org/10.1103/PhysRevD.91.043520. URL: https://link.aps.org/doi/10.1103/PhysRevD.91.043520.

[21] P. Pirinen, P.C. Srivastava, J. Suhonen, M. Kortelainen, Shell-model study on event rates of lightest supersymmetric particles scattering off ^{83}Kr and ^{125}Te, Phys. Rev. D 93 (2016) 095012, https://doi.org/10.1103/PhysRevD.93.095012. URL: https://link.aps.org/doi/10.1103/PhysRevD.93.095012.

[22] A.L. Fitzpatrick, W. Haxton, E. Katz, N. Lubbers, Y. Xu, The effective field theory of dark matter direct detection, J. Cosmol. Astropart. Phys. 2013 (02) (2013) 004, https://doi.org/10.1088/1475-7516/2013/02/004. URL: https://doi.org/10.1088/1475-7516/2013/02/004.

[23] F. Iachello, P. van Isacker, The Interacting Boson-Fermion Model, Cambridge Monographs on Mathematical Physics, Cambridge University Press, 1991.

[24] F. Iachello, L.M. Krauss, G. Maino, Spin-dependent scattering of weakly interacting massive particles in heavy nuclei, Phys. Lett. B 254 (1) (1991) 220–224, https://doi.org/10.1016/0370-2693(91)90424-O. URL: http://www.sciencedirect.com/science/article/pii/037026939190424O.

[25] CRESST collaboration, Petricca F., G. Angloher, P. Bauer, A. Bento, C. Bucci, et al., First results on low-mass dark matter from the CRESST-III experiment, arXiv e-prints, arXiv:1711.07692, 2017.

[26] V. Bernard, N. Kaiser, U.G. Meißner, Aspects of chiral pion-nucleon physics, Nucl. Phys. A 615 (4) (1997) 483–500, https://doi.org/10.1016/S0375-9474(97)00021-3. URL: http://www.sciencedirect.com/science/article/pii/S0375947497000213.

[27] D.R. Entem, R. Machleidt, Accurate charge-dependent nucleon-nucleon potential at fourth order of chiral perturbation theory, Phys. Rev. C 68 (2003) 041001, https://doi.org/10.1103/PhysRevC.68.041001. URL: https://link.aps.org/doi/10.1103/PhysRevC.68.041001.

[28] E. Epelbaum, W. Glöckle, U.G. Meißner, The two-nucleon system at next-to-next-to-next-to-leading order, Nucl. Phys. A 747 (2) (2005) 362–424, https://doi.org/10.1016/j.nuclphysa.2004.09.107. URL: http://www.sciencedirect.com/science/article/pii/S0375947404010747.

[29] M.C.M. Rentmeester, R.G.E. Timmermans, J.J. de Swart, Determination of the chiral coupling constants c_3 and c_4 in new pp and np partial-wave analyses, Phys. Rev. C 67 (2003) 044001, https://doi.org/10.1103/PhysRevC.67.044001. URL: https://link.aps.org/doi/10.1103/PhysRevC.67.044001.

[30] E. Epelbaum, H.W. Hammer, U.G. Meißner, Modern theory of nuclear forces, Rev. Mod. Phys. 81 (2009) 1773–1825, https://doi.org/10.1103/RevModPhys.81.1773. URL: https://link.aps.org/doi/10.1103/RevModPhys.81.1773.

[31] G. Puddu, O. Scholten, T. Otsuka, Collective quadrupole states of Xe, Ba and Ce in the interacting boson model, Nucl. Phys. A 348 (1) (1980) 109–124, https://doi.org/10.1016/0375-9474(80)90548-5. URL: http://www.sciencedirect.com/science/article/pii/0375947480905485.

[32] M. Sambataro, A study of Cd and Te isotopes in the interacting boson approximation, Nucl. Phys. A 380 (3) (1982) 365–382, https://doi.org/10.1016/0375-9474(82)90565-6. URL: http://www.sciencedirect.com/science/article/pii/0375947482905656.

[33] J. Kotila, J. Barea, Occupation probabilities of single particle levels using the microscopic interacting boson model: application to some nuclei of interest in neutrinoless double-β decay, Phys. Rev. C 94 (2016) 034320, https://doi.org/10.1103/PhysRevC.94.034320. URL: https://link.aps.org/doi/10.1103/PhysRevC.94.034320.

[34] J. Barea, C. Alonso, J. Arias, The one nucleon transfer operator in the microscopic IBM without NOA, Phys. Lett. B 737 (2014) 205–209, https://doi.org/10.1016/j.physletb.2014.08.026. URL: http://www.sciencedirect.com/science/article/pii/S0370269314005930.

[35] A. Arima, T. Ohtsuka, F. Iachello, I. Talmi, Collective nuclear states as symmetric couplings of proton and neutron excitations, Phys. Lett. B 66 (3) (1977) 205–208, https://doi.org/10.1016/0370-2693(77)90860-7. URL: http://www.sciencedirect.com/science/article/pii/0370269377908607.

[36] T. Otsuka, A. Arima, F. Iachello, Nuclear shell model and interacting bosons, Nucl. Phys. A 309 (1) (1978) 1–33, https://doi.org/10.1016/0375-9474(78)90532-8. URL: http://www.sciencedirect.com/science/article/pii/0375947478905328.

[37] J. Barea, F. Iachello, Neutrinoless double-β decay in the microscopic interacting boson model, Phys. Rev. C 79 (2009) 044301, https://doi.org/10.1103/PhysRevC.79.044301. URL: https://link.aps.org/doi/10.1103/PhysRevC.79.044301.

[38] National nuclear data center, evaluated nuclear structure data file, https://www.nndc.bnl.gov/ensdf/, 2019. (Accessed 15 May 2019).

[39] J.D. Vergados, F.T. Avignone III, M. Kortelainen, P. Pirinen, P.C. Srivastava, J. Suhonen, et al., Inelastic WIMP-nucleus scattering to the first excited state in ^{125}Te, J. Phys. G, Nucl. Part. Phys. 43 (11) (2016) 115002, https://doi.org/10.1088/0954-3899/43/11/115002. URL: https://doi.org/10.1088/0954-3899/43/11/115002.

[40] E. Aprile, J. Aalbers, F. Agostini, M. Alfonsi, L. Althueser, F.D. Amaro, et al., XENON Collaboration, Dark matter search results from a one ton-year exposure of XENON1T, Phys. Rev. Lett. 121 (2018) 111302, https://doi.org/10.1103/PhysRevLett.121.111302. URL: https://link.aps.org/doi/10.1103/PhysRevLett.121.111302.

[41] K. Abe, K. Hiraide, K. Ichimura, Y. Kishimoto, K. Kobayashi, M. Kobayashi, et al., XMASS Collaboration, Direct dark matter search by annual modulation with 2.7 years of XMASS-I data, Phys. Rev. D 97 (2018) 102006, https://doi.org/10.1103/PhysRevD.97.102006. URL: https://link.aps.org/doi/10.1103/PhysRevD.97.102006.

[42] D.S. Akerib, C.W. Akerlof, S.K. Alsum, H.M. Araújo, M. Arthurs, X. Bai, et al., Projected WIMP sensitivity of the LUX-ZEPLIN (LZ) dark matter experiment, arXiv e-prints, arXiv:1802.06039, 2018.

[43] X. Cui, A. Abdukerim, W. Chen, X. Chen, Y. Chen, B. Dong, et al., PandaX-II Collaboration, Dark matter results from 54-ton-day exposure of PandaX-II experiment, Phys. Rev. Lett. 119 (2017) 181302, https://doi.org/10.1103/PhysRevLett.119.181302. URL: https://link.aps.org/doi/10.1103/PhysRevLett.119.181302.

[44] N. Anand, A.L. Fitzpatrick, W.C. Haxton, Weakly interacting massive particle-nucleus elastic scattering response, Phys. Rev. C 89 (2014) 065501, https://doi.org/10.1103/PhysRevC.89.065501. URL: https://link.aps.org/doi/10.1103/PhysRevC.89.065501.